

LETTER TO THE EDITOR

Discovering extremely compact and metal-poor, star-forming dwarf galaxies out to $z \sim 0.9$ in the VIMOS Ultra-Deep Survey*

R. Amorín¹, V. Sommariva^{5,1}, M. Castellano¹, A. Grazian¹, L. A. M. Tasca², A. Fontana¹, L. Pentericci¹, P. Cassata², B. Garilli⁴, V. Le Brun², O. Le Fèvre², D. Maccagni⁴, R. Thomas², E. Vanzella³, G. Zamorani³, E. Zucca³, S. Bardelli³, P. Capak¹², L. P. Cassará⁴, A. Cimatti⁵, J.G. Cuby², O. Cucciati^{5,3}, S. de la Torre², A. Durkalec², M. Giavalisco¹³, N. P. Hathi², O. Ilbert², B. C. Lemaux², C. Moreau², S. Paltani⁹, B. Ribeiro², M. Salvato¹⁴, D. Schaefer^{10,8}, M. Scudiego⁴, M. Talia⁵, Y. Taniguchi¹⁵, L. Tresse², D. Vergani^{6,3}, P.W. Wang², S. Charlot⁷, T. Contini⁸, S. Fotopoulou⁹, C. López-Sanjuan¹¹, Y. Mellier⁷, and N. Scoville¹²

(Affiliations can be found after the references)

ABSTRACT

We report the discovery of 31 low-luminosity ($-14.5 \gtrsim M_{AB}(B) \gtrsim -18.8$), extreme emission line galaxies (EELGs) at $0.2 \lesssim z \lesssim 0.9$ identified by their unusually high rest-frame equivalent widths ($100 \leq \text{EW}[\text{O III}] \leq 1700 \text{\AA}$) as part of the VIMOS Ultra Deep Survey (VUDS). VIMOS optical spectra of unprecedented sensitivity ($I_{AB} \sim 25$ mag) along with multiwavelength photometry and HST imaging are used to investigate spectrophotometric properties of this unique sample and to explore, for the first time, the very low stellar mass end ($M_\star \lesssim 10^8 M_\odot$) of the luminosity-metallicity (LZR) and mass-metallicity (MZR) relations at $z < 1$. Characterized by their extreme compactness ($R_{50} < 1$ kpc), low stellar mass and enhanced specific star formation rates ($\text{sSFR} = \text{SFR}/M_\star \sim 10^{-9} - 10^{-7} \text{ yr}^{-1}$), the VUDS EELGs are blue dwarf galaxies likely experiencing the first stages of a vigorous galaxy-wide starburst. Using T_e -sensitive *direct* and strong-line methods, we find that VUDS EELGs are low-metallicity ($7.5 \lesssim 12 + \log(\text{O/H}) \lesssim 8.3$) galaxies with high ionization conditions ($\log(q_{\text{ion}}) \gtrsim 8 \text{ cm s}^{-1}$), including at least three EELGs showing $\text{He I} \lambda 4686 \text{\AA}$ emission and four extremely metal-poor ($\lesssim 10\%$ solar) galaxies. The LZR and MZR followed by VUDS EELGs show relatively large scatter, being broadly consistent with the extrapolation toward low luminosity and mass from previous studies at similar redshift. However, we find evidence that galaxies with younger and more vigorous star formation – as characterized by their larger EWs, ionization and sSFR – tend to be more metal poor at a given stellar mass.

Key words. galaxies : evolution – galaxies : high redshift – galaxies : dwarfs – galaxies : abundances – galaxies : starbursts

1. Introduction

Over the last 8 billion years a large fraction of low-mass ($M_\star \lesssim 10^9 M_\odot$) galaxies are still seen rapidly assembling most of their present-day stellar mass (Cowie et al. 1996; Pérez-González et al. 2008). Tracing the spectrophotometric properties of these vigorous star-forming *dwarf* galaxies (SFDGs) out to $z \sim 1$ is essential not only to study how they evolve through cosmic time, but also to understand the physical mechanisms driving the first stages of stellar mass build-up and chemical enrichment. To this end, key insights can be obtained from the tight relations found between stellar mass, metallicity and star formation rate (SFR). However, the shape and normalization of these relations at different redshifts are still poorly constrained at their low-mass end. While in the local Universe the mass-metallicity relation (MZR) has been extended down to $10^8 M_\odot$ (e.g. Andrews & Martini 2013), at intermediate and high redshifts, dwarf galaxies are strongly underrepresented (e.g. Henry et al. 2013).

These SFDGs are usually identified by their blue colors, high surface brightness and strong emission-lines. They include a rare population of extreme emission-line galaxies (EELGs) with the largest nebular content and lowest metal abundances (e.g. Kniazev et al. 2004; Papaderos et al. 2008; Hu et al. 2009;

Atek et al. 2011; Morales-Luis et al. 2011). Due to their high equivalent widths (EWs), an increasing number of EELGs are being discovered and characterized by deep spectroscopic surveys out to $z \sim 1$ (e.g. Hoyos et al. 2005; Ly et al. 2014; Amorín et al. 2014a) and beyond (e.g. van der Wel et al. 2011; Maseda et al. 2014). In this *Letter* we report the discovery of a sample of 31 EELGs at $0.2 \lesssim z \lesssim 0.9$ identified from the *VIMOS Ultra-Deep Survey* (VUDS; Le Fevre et al. 2014). We study their physical properties as part of a larger, ongoing study aimed at investigating the evolution of SFDGs out to $z \sim 1$ using very deep spectroscopy (e.g. Amorín et al. 2014a). The sensitivity of our VUDS spectra, detecting emission lines as faint as $\sim 1.5 \times 10^{-18} \text{ erg s}^{-1} \text{ cm}^{-2}$, makes it possible e.g., to derive T_e -based metallicities for a fraction of such faint galaxies. Thus, the present sample extends previous studies of star-forming (SF) galaxies at similar redshifts in size and limiting magnitude (Henry et al. 2013; Ly et al. 2014), allowing us to study in greater detail the LZR and MZR at $z < 1$ two decades below $10^9 M_\odot$ with galaxies showing a wide range of properties, including a number of extremely metal-poor galaxies. Throughout this paper we adopt a standard Λ -CDM cosmology with $h = 0.7$, $\Omega_m = 0.3$ and $\Omega_\Lambda = 0.7$.

2. Observations and sample selection

The *Vimos Ultra Deep Survey* is a deep spectroscopic legacy survey of $\sim 10^4$ galaxies carried out using VIMOS at ESO-VLT

* Based on data obtained with the European Southern Observatory Very Large Telescope, Paranal, Chile, under Large Program 185.A-0791.

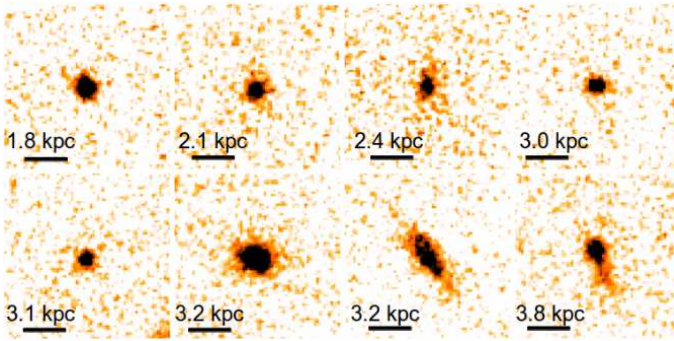


Fig. 1: HST $F814W$ -band imagery of EELGs in the COSMOS and ECDF fields covered by VUDS. Each postage stamp is $2''$ on a side.

(Le Fèvre et al. 2003). This survey is aimed at providing a complete census of the SF galaxy population at $2 \lesssim z \lesssim 7$, covering $\sim 1 \text{ deg}^2$ in three fields: COSMOS, ECDFS, and VVDS-2h. The VIMOS spectra consist of 14h integrations in the LRBLUE and LRRED grism settings, covering a combined wavelength range $3650 < \lambda < 9350\text{\AA}$, with a spectral resolution $R \sim 230$. Data reduction, redshift measurement, and assessment of the reliability flags are described in detail in the survey and data presentation paper (Le Fevre et al. 2014).

The targets of VUDS have been primarily selected to have photometric redshifts $z_p > 2.4$ for either of the primary and secondary peaks of the PDF. A number of random targets purely magnitude selected to $23 \leq I_{AB} \leq 25$ have been added to fill empty areas on observed slit masks. As a consequence, we identify a number of targets with spectroscopic redshift $z_s < 2$. Many of these targets are galaxies with prominent optical emission lines, such as $[\text{O II}]\lambda 3727$ or $[\text{O III}]\lambda 5007$, that artificially boost the observed magnitudes in the stellar spectral energy distributions (SED).

For this *Letter* a representative sample of 31 EELGs (12 from COSMOS, 11 from VVDS-2h, and 8 from ECDFS) with mean $I_{AB} \sim 24.5$ mag was identified from an early version of VUDS data containing $\sim 40\%$ of the final sample. We first consider primary and secondary target galaxies with very reliable spectroscopic redshift (98% and 100% confidence level), at $z \leq 0.93$. We then select galaxies with at least three emission lines detected, $[\text{O II}]$, $[\text{O III}]$, and $\text{H}\beta$, and $\text{EW}[\text{O III}] > 100\text{\AA}$. The first criterion ensures the derivation of gas-phase metallicities and the second allows us to select SFDGs with the highest *specific* SFR (e.g. Atek et al. 2011; Ly et al. 2014; Amorín et al. 2014a).

While our EELGs look unresolved in ground-based images precluding a full morphological analysis, morphological information can be obtained for a subset of 16 EELGs that have been observed by the HST-ACS in the $F814W$ (I) band. As illustrated in Fig. 1, EELGs include galaxies with both round and irregular shapes, showing angular sizes $< 1''$. Using the automated method presented in Tasca et al. (2009) for the EELGs imaged by the ACS we derive circularized half-light radii, $r_{50} = R_{50}(b/a)^{0.5} \sim 0.4\text{--}0.8 \text{ kpc}$ thus confirming their extreme compactness. In most cases, we find these EELGs with no clear signs of ongoing mergers or very close companions.

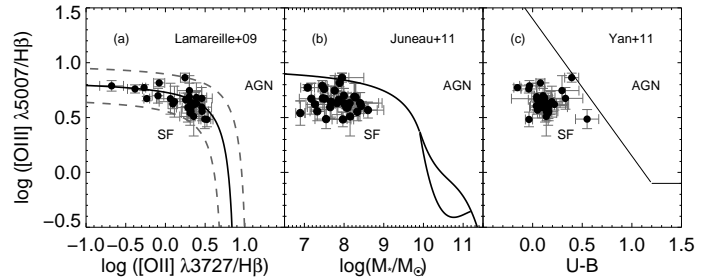


Fig. 2: Diagnostic diagrams. Lines show the empirical separations between SF galaxies and AGNs.

3. Physical properties of VUDS EELGs

Deep VUDS spectra for the sample of EELGs are presented in Fig. A.1¹. Long exposure times allow us to detect in most cases a remarkably faint continuum ($\sim 5 \times 10^{-20} \text{ erg s}^{-1} \text{ cm}^2 \text{\AA}^{-1}$, 1σ) and very faint lines, such as $[\text{O III}]\lambda 4363$ or $[\text{N II}]\lambda 6584$. In Table 1² we present line fluxes and uncertainties for the most relevant detected emission lines, which were performed manually using the IRAF task *splot* following Amorín et al. (2012). Reddening corrections were performed using the Balmer decrement, whenever available, and adopting the Calzetti et al. (2000) extinction law. For those EELGs with $\text{H}\alpha/\text{H}\beta$ or $\text{H}\beta/\text{H}\gamma$ measurements the median reddening is $E(B-V)_{\text{gas}}^{\text{med}} = 0.26$ ($\sigma = 0.14$), in good agreement with previous studies for EELGs (e.g., Domínguez et al. 2013; Ly et al. 2014; Amorín et al. 2014a). In those cases where $E(B-V)_{\text{gas}}$ cannot be measured through $\text{H}\alpha/\text{H}\beta$ or $\text{H}\beta/\text{H}\gamma$, or where its values are smaller than the theoretical values for the Case B recombination ($T_e = 2 \times 10^4 \text{ K}$, $n_e = 100 \text{ cm}^{-3}$), we adopt $E(B-V)_{\text{gas}} = E(B-V)_*$, where $E(B-V)_*$ is the stellar extinction derived from the SED fitting described in Section 3.2. This assumption seems reasonable since median values of stellar $(E(B-V))_{\star}^{\text{med}} = 0.25$, $\sigma = 0.14$) and gas extinctions are in excellent agreement for galaxies for which both values are available. The adopted reddening constant for each galaxy is listed in Table 1. In the following sections we describe the derivation of the main physical properties for the EELG sample, which are presented in Table 2².

3.1. Ionization and metallicity properties from VUDS spectra

In Figure 2 we study the ionization properties of the EELG sample using three diagnostic diagrams based on strong emission line ratios. Our sample galaxies populate the region of SF galaxies with the highest excitation ($[\text{O III}]/\text{H}\beta \sim 5 \pm 2$). Consistently with their low masses and blue $U - B$ colors, none of them shows indication of an Active Galactic Nuclei (AGN) activity. Our EELGs, however, are located near the limits between SF and AGN regions in Fig. 2 due to their high ionization conditions, as suggested by their high $[\text{O III}]/[\text{O II}]$ ratios (Fig. 2a). In the most extreme case, $[\text{O III}]$ shows EW of $\sim 1700\text{\AA}$, while the $[\text{O II}]$ line is only barely detected. Moreover, in three EELGs, we tentatively detect ($\sim 2.5\sigma$) $\text{He II} 4686\text{\AA}$ emission, suggesting the presence of very young, hot stars. Being rare at $z < 1$ (e.g., Jaskot & Oey 2013; Nakajima & Ouchi 2014; Amorín et al. 2014a), these EELGs show ionization parameters ($\log(q_{\text{ion}}) \gtrsim 8 \text{ cm s}^{-1}$) comparable to some low-luminosity

¹ Only available in the electronic edition of the journal

² Tables 1 and 2 are only available in electronic form at the CDS via <http://cdsweb.u-strasbg.fr/cgi-bin/qcat?J/A+A/>

high redshift galaxies (e.g., Fosbury et al. 2003; Amorín et al. 2014b).

In seven EELGs we detect ($\geq 2\sigma$) the intrinsically faint T_e -sensitive auroral line [O III] $\lambda 4363\text{\AA}$. For these galaxies we derive metallicity using the direct method (Hägele et al. 2008). In addition, we derive metallicities for the entire sample using the $R23(\equiv \text{[O II} + \text{O III}]/\text{H}\beta)$ parameter and the calibration of McGaugh (1991). Following Pérez-Montero et al. (2013) we apply the linear relations detailed in Lamareille et al. (2006) to make these $R23$ metallicities consistent with those derived using the direct method. In order to break the degeneracy of $R23$ (i.e., to choose between the lower or upper branch) we use two additional indicators. For EELGs at $z \lesssim 0.45$ we choose the branch that best matches the metallicity obtained from the $N2(\equiv \text{N II}/\text{H}\alpha)$ parameter and the calibration by Pérez-Montero & Contini (2009), while for EELGs at $z \gtrsim 0.45$ we choose the branch that best matches the metallicity from the calibrations based on the [Ne III], [O II], and [O III] line ratios of Maiolino et al. (2008). The difference between direct and strong-line metallicity estimations for the seven galaxies with [O III] $\lambda 4363\text{\AA}$ is < 0.2 dex. We find the metallicity of our EELG spanning a wide range of subsolar values ($7.5 \lesssim 12 + \log(\text{O/H}) \lesssim 8.3$), including four extremely metal-poor galaxies ($Z \lesssim 0.1 Z_\odot$).

3.2. Stellar properties from multiwavelength SED fitting

Stellar masses and rest-frame absolute magnitudes of EELGs were derived by fitting their stellar SEDs. In short, we fit Bruzual & Charlot (2003) stellar population synthesis models to the broad-band photometry – from UV to NIR – of each galaxy using chi-square minimization following Castellano et al. (2014). Magnitudes are previously corrected from the contribution of prominent optical emission lines following Amorín et al. (2014a), while models assume stellar metallicities that best agree with the observed gas-phase metallicity. We adopt a Chabrier (2003) IMF, Calzetti et al. (2000) extinction law and assume a standard declining exponential star formation history. As a result, we find the sample of EELGs in VUDS spanning a range of low luminosities, $-14.5 \lesssim M_{AB}(B) \lesssim -18.8$, and low stellar masses, $6.9 \lesssim \log(M_*/M_\odot) \lesssim 8.6$.

4. The relation between mass, metallicity, and ongoing SFR of low-mass galaxies out to $z \sim 1$

In Fig. 3 we show the SFR-mass diagram for the EELGs in VUDS and from the literature. Star formation rates are derived from the extinction-corrected H α or H β luminosities using the calibration of Kennicutt (1998) and assuming a Chabrier (2003) IMF. At a given redshift, our EELGs show SFRs and stellar masses a factor of ~ 10 lower than similar samples from the literature. However, nearly all EELGs shown in Fig. 3 are well above the extrapolation to low stellar mass of the main sequence of galaxies (Whitaker et al. 2012) at a given z . The EELGs in VUDS show enhanced specific SFRs (sSFR $\sim 10^{-9}$ - 10^{-7} yr $^{-1}$) and SFR surface densities (median $\Sigma_{\text{SFR}} = \text{SFR}/2\pi r_{50}^2 = 0.35$ ($\sigma = 0.19$) $M_\odot \text{ yr}^{-1} \text{ kpc}^{-2}$), comparable to more luminous galaxy-wide starbursts at similar and higher redshifts (Ly et al. 2014; Amorín et al. 2014a,b).

In Fig. 4 we study the LZR and MZR traced by EELGs in VUDS and other low-mass galaxies at $0 < z < 1$. The EELGs extend the LZR down to $M_{AB}(B) \sim -14.5$ and the MZR down to $M_* \sim 10^7 M_\odot$, which means ~ 1 dex lower than previ-

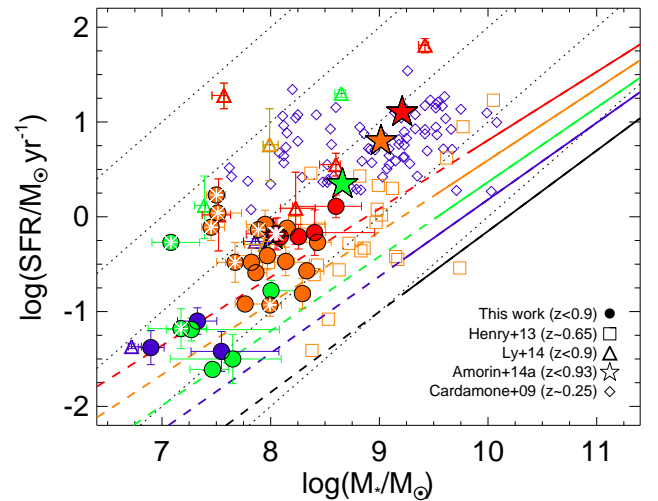


Fig. 3: The SFR stellar mass plane of low-mass SFDGs. Solid and dashed lines show the so-called main sequence of galaxies at different redshifts and its extrapolation to low-mass regime, respectively, according to Whitaker et al. (2012). Dotted lines indicate constant sSFR from 10^{-10} yr $^{-1}$ (bottom) to 10^{-6} yr $^{-1}$ (upper). Colors indicate redshift bins with mean values $\langle z \rangle = 0$ (black), $\langle z \rangle = 0.25$ (blue), $\langle z \rangle = 0.4$ (green), $\langle z \rangle = 0.6$ (orange) and $\langle z \rangle = 0.8$ (red). Asterisks show VUDS EELGs with $\text{EW}_{\text{rest}}(\text{O III}) > 200\text{\AA}$ and $\text{EW}_{\text{rest}}(\text{H}\beta) > 60\text{\AA}$.

ous studies (e.g., Henry et al. 2013), thus increasing substantially the number of low-mass galaxies under study, especially at $z \gtrsim 0.5$. Despite the relatively large scatter, VUDS EELGs appear to follow the LZR and MZR of more luminous and massive SFDGs. In particular, we find most EELGs in broad agreement with the local ($z < 0.3$) LZR of Guseva et al. (2009) and MZR of Andrews & Martini (2013), which have been derived from galaxies with T_e -based metallicities. There is nevertheless a tendency for EELGs with larger EWs to be more metal-poor at a given luminosity, stellar mass, and redshift. These galaxies are those with the highest sSFR, i.e., those with the largest deviations from the main sequence of star formation at a given z , shown in Fig. 3. While they follow more reliably the LZR traced by extremely metal-poor galaxies (e.g., Kewley et al. 2007; Hu et al. 2009), they tend to lie below the local MZR, similarly to other extreme galaxies (see, e.g., the *green peas* Amorín et al. 2010).

Part of the above apparent dependence of the MZR on SFR can be explained in terms of the fundamental metallicity relation (FMR; Mannucci et al. 2010), which suggests that galaxies with higher sSFR tend to be more metal-poor at a given stellar mass. As shown in Fig. 4, the position of the VUDS EELGs appears broadly consistent with the extrapolation to low masses of the FMR, independently of the parametrization and metallicity scale adopted. We notice, however, that the scatter in the FMR for EELGs ($\sigma \sim 0.20$) seems slightly larger than expected for magnitude-selected samples in the local universe.

Overall, the above results are consistent with a picture where the most extreme SFDGs are very gas-rich galaxies experiencing an early stage of a galaxy-wide starburst, possibly fed by recent accretion of metal-poor gas (e.g., Amorín et al. 2010; Sánchez Almeida et al. 2014). In this picture, at least part of the scatter in the above scaling relations could be produced by differences in the accretion and star formation histories.

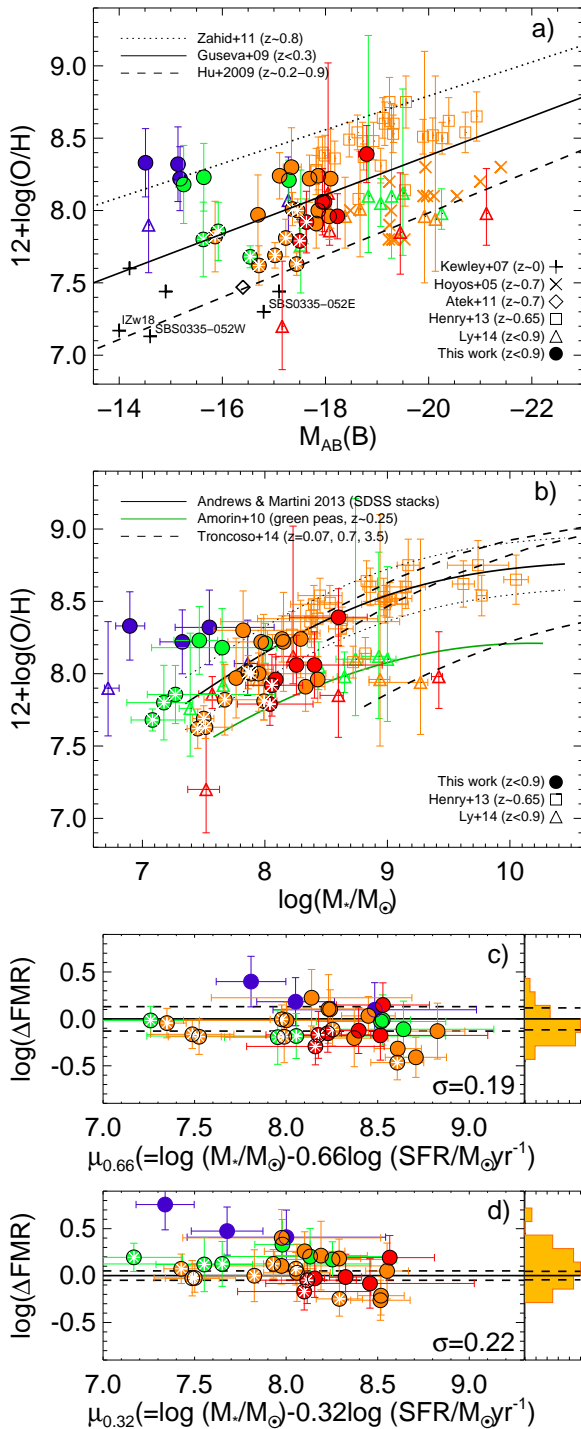


Fig. 4: (a) Luminosity-metalllicity and (b) mass-metalllicity relations for VUDS EELGs and SFDGs from the literature. Metallicity differences with respect to the extrapolation to low stellar mass of the FMR by Andrews & Martini (2013) and Mannucci et al. (2011) are shown in (c) and (d), respectively. Dashed lines indicate 1σ deviations for these relations. Colors and symbols are as in Fig. 3. The data have been homogenized to the Chabrier IMF and the same strong-line metallicity calibration presented in Section 3.1.

Figure 4 also suggests that the shape of the MZR can be very sensitive to selection effects in its very low-mass end. Gas-rich dwarfs with prominent emission lines, enhanced sSFR and low

metallicities may be overrepresented with respect to the global population of SFDGs in magnitude-selected spectroscopic samples at these redshifts, making the shape of the MZR at low mass not entirely representative of main sequence galaxies. Clearly, a thorough study using the deepest spectroscopy available for a statistical significant complete sample of SFDGs is much needed to test this hypothesis. Forthcoming analysis of VUDS galaxies at $z < 1$ using the complete database will enable us to scrutinize in detail the underexplored low-mass universe at $z < 1$.

Acknowledgements. We thank the anonymous referee for helpful comments that helped to improve this manuscript. We thank the ESO staff for their continuous support for the VUDS survey, particularly the Paranal staff conducting the observations and Marina Rejkuba and the ESO user support group in Garching. This work is supported by funding from the European Research Council Advanced Grant ERC-2010-AdG-268107-EARLY and by INAF Grants PRIN 2010, PRIN 2012 and PICS 2013. RA and AF acknowledge the FP7 SPACE project ASTRODEEP (Ref.No: 312725), supported by the European Commission. AC, OC, MT and VS acknowledge the grant MIUR PRIN 2010–2011. DM gratefully acknowledges LAM hospitality during the initial phases of the project. This work is based on data products made available at the CESAM data center, Laboratoire d’Astrophysique de Marseille. This work partly uses observations obtained with MegaPrime/MegaCam, a joint project of CFHT and CEA/DAPNIA, at the Canada-France-Hawaii Telescope (CFHT) which is operated by the National Research Council (NRC) of Canada, the Institut National des Sciences de l’Univers of the Centre National de la Recherche Scientifique (CNRS) of France, and the University of Hawaii. This work is based in part on data products produced at TERAPIX and the Canadian Astronomy Data Centre as part of the Canada-France-Hawaii Telescope Legacy Survey, a collaborative project of NRC and CNRS.

References

- Amorín, R. O., Pérez-Montero, E., & Vilchez, J. M. 2010, ApJ, 715, L128
- Amorín, R., Pérez-Montero, E., Vilchez, J. M., & Papaderos, P. 2012, ApJ, 749, 185
- Amorín, R., Pérez-Montero, E., Contini, T., et al. 2014a, arXiv:1403.3441
- Amorín, R., Grazian, A., Castellano, M., et al. 2014b, ApJ, 788, L4
- Andrews, B. H., & Martini, P. 2013, ApJ, 765, 140
- Atek, H., Siana, B., Scarlata, C., et al. 2011, ApJ, 743, 121
- Bruzual, G. & Charlot, S. 2003, MNRAS, 344, 1000
- Calzetti, D., Armus, L., Bohlin, R. C., et al. 2000, ApJ, 533, 682
- Cardamone, C., Schawinski, K., Sarzi, M., et al. 2009, MNRAS, 399, 1191
- Castellano, M., Sommariva, V., Fontana, A., et al. 2014, A&A, 566, A19
- Cowie, L. L., Songaila, A., Hu, E. M., & Cohen, J. G. 1996, AJ, 112, 839
- Chabrier, G. 2003, PASP, 115, 763
- Domínguez, A., Siana, B., Henry, A. L., et al. 2013, ApJ, 763, 145
- Fossey, R. A. E., Villar-Martín, M., Humphrey, A., et al. 2003, ApJ, 596, 797
- Guseva, N. G., Papaderos, P., Meyer, H. T., et al. 2009, A&A, 505, 63
- Hägele, G. F., Díaz, Á. I., Terlevich, E., et al. 2008, MNRAS, 383, 209
- Henry, A., Martin, C. L., Finlator, K., & Dressler, A. 2013, ApJ, 769, 148
- Hoyos, C., Koo, D. C., Phillips, et al. 2005, ApJ, 635, L21
- Hu, E. M., Cowie, L. L., Kakazu, Y., & Barger, A. J. 2009, ApJ, 698, 2014
- Jaskot, A. E., & Oey, M. S. 2013, ApJ, 766, 91
- Juneau, S., Dickinson, M., Alexander, D. M., & Salim, S. 2011, ApJ, 736, 104
- Kennicutt, R. C., Jr. 1998, ApJ, 498, 541
- Kewley, L. J., Brown, W. R., Geller, M. J., Kenyon, S. J., & Kurtz, M. J. 2007, AJ, 133, 882
- Kniazev, A. Y., Pustilnik, S. A., Grebel, E. K., Lee, H., & Pramskij, A. G. 2004, ApJS, 153, 429
- Lamareille, F., Contini, T., Brinchmann, J., et al. 2006b, A&A, 448, 907
- Lamareille, F., Brinchmann, J., Contini, T., et al. 2009, A&A, 495, 53
- Le Fèvre, O., Saisse, M., Mancini, D., et al. 2003, Proc. SPIE, 4841, 1670
- Le Fevre, O., Tasca, L. A. M., Cassata, P., et al. 2014, arXiv:1403.3938
- Ly, C., Malkan, M. A., Nagao, T., et al. 2014, ApJ, 780, 122
- Maiolino, R., Nagao, T., Grazian, A., et al. 2008, A&A, 488, 463
- Mannucci, F., Cresci, G., Maiolino, R., Marconi, A., & Gnerucci, A. 2010, MNRAS, 408, 2115
- Mannucci, F., Salvaterra, R., & Campisi, M. A. 2011, MNRAS, 414, 1263
- Maseda, M. V., van der Wel, A., Rix, H.-W., et al. 2014, arXiv:1406.3351
- McGaugh, S. S. 1991, ApJ, 380, 140
- Morales-Luis, A. B., Sánchez Almeida, J., Aguerri, J. A. L., & Muñoz-Tuñón, C. 2011, ApJ, 743, 77
- Nakajima, K., & Ouchi, M. 2014, MNRAS, 442, 900
- Papaderos, P., Guseva, N. G., Izotov, Y. I., & Fricke, K. J. 2008, A&A, 491, 113

- Pérez-Montero, E. & Díaz, A.I. 2003, MNRAS, 346, 105.
Pérez-Montero, E. & Contini, T. 2009, MNRAS, 398, 949
Pérez-Montero, E., Contini, T., Lamareille, F., et al. 2013, A&A, 549, A25
Pérez-González, P. G., Rieke, G. H., Villar, V., et al. 2008, ApJ, 675, 234
Sánchez Almeida, J., Morales-Luis, A. B., et al. 2014, ApJ, 783, 45
Tasca, L. A. M., Kneib, J.-P., Iovino, A., et al. 2009, A&A, 503, 379
Troncoso, P., Maiolino, R., Sommariva, V., et al. 2014, A&A, 563, A58
van der Wel, A., Straughn, A. N., Rix, H.-W., et al. 2011, ApJ, 742, 111
Whitaker, K. E., van Dokkum, P. G., Brammer, G., & Franx, M. 2012, ApJ, 754,
L29
Yan, R., Ho, L. C., Newman, J. A., et al. 2011, ApJ, 728, 38
Zahid, H. J., Kewley, L. J., & Bresolin, F. 2011, ApJ, 730, 137

-
- ¹ INAF–Osservatorio Astronomico di Roma, via di Frascati 33, I-00040, Monte Porzio Catone, Italy
- ² Aix Marseille Université, CNRS, LAM (Laboratoire d’Astrophysique de Marseille) UMR 7326, 13388, Marseille, France
- ³ INAF–Osservatorio Astronomico di Bologna, via Ranzani, 1, I-40127, Bologna, Italy
- ⁴ INAF–IASF, via Bassini 15, I-20133, Milano, Italy
- ⁵ University of Bologna, Department of Physics and Astronomy (DIFA), V.le Berti Pichat, 6/2 - 40127, Bologna
- ⁶ INAF–IASF Bologna, via Gobetti 101, I-40129, Bologna, Italy
- ⁷ Institut d’Astrophysique de Paris, UMR7095 CNRS, Université Pierre et Marie Curie, 98 bis Boulevard Arago, 75014, Paris, France
- ⁸ Institut de Recherche en Astrophysique et Planétologie - IRAP, CNRS, Université de Toulouse, UPS-OMP, 14, avenue E. Belin, F31400, Toulouse, France
- ⁹ Department of Astronomy, University of Geneva, ch. d’cogia 16, CH-1290 Versoix
- ¹⁰ Geneva Observatory, University of Geneva, ch. des Maillettes 51, CH-1290 Versoix, Switzerland
- ¹¹ Centro de Estudios de Física del Cosmos de Aragón, Teruel, Spain
- ¹² Department of Astronomy, California Institute of Technology, 1200 E. California Blvd., MC 249-17, Pasadena, CA 91125, USA
- ¹³ Astronomy Department, University of Massachusetts, Amherst, MA 01003, USA
- ¹⁴ Max-Planck-Institut für Extraterrestrische Physik, Postfach 1312, D-85741, Garching bei München, Germany
- ¹⁵ Research Center for Space and Cosmic Evolution, Ehime University, Bunkyo-cho 2-5, Matsuyama 790-8577, Japan

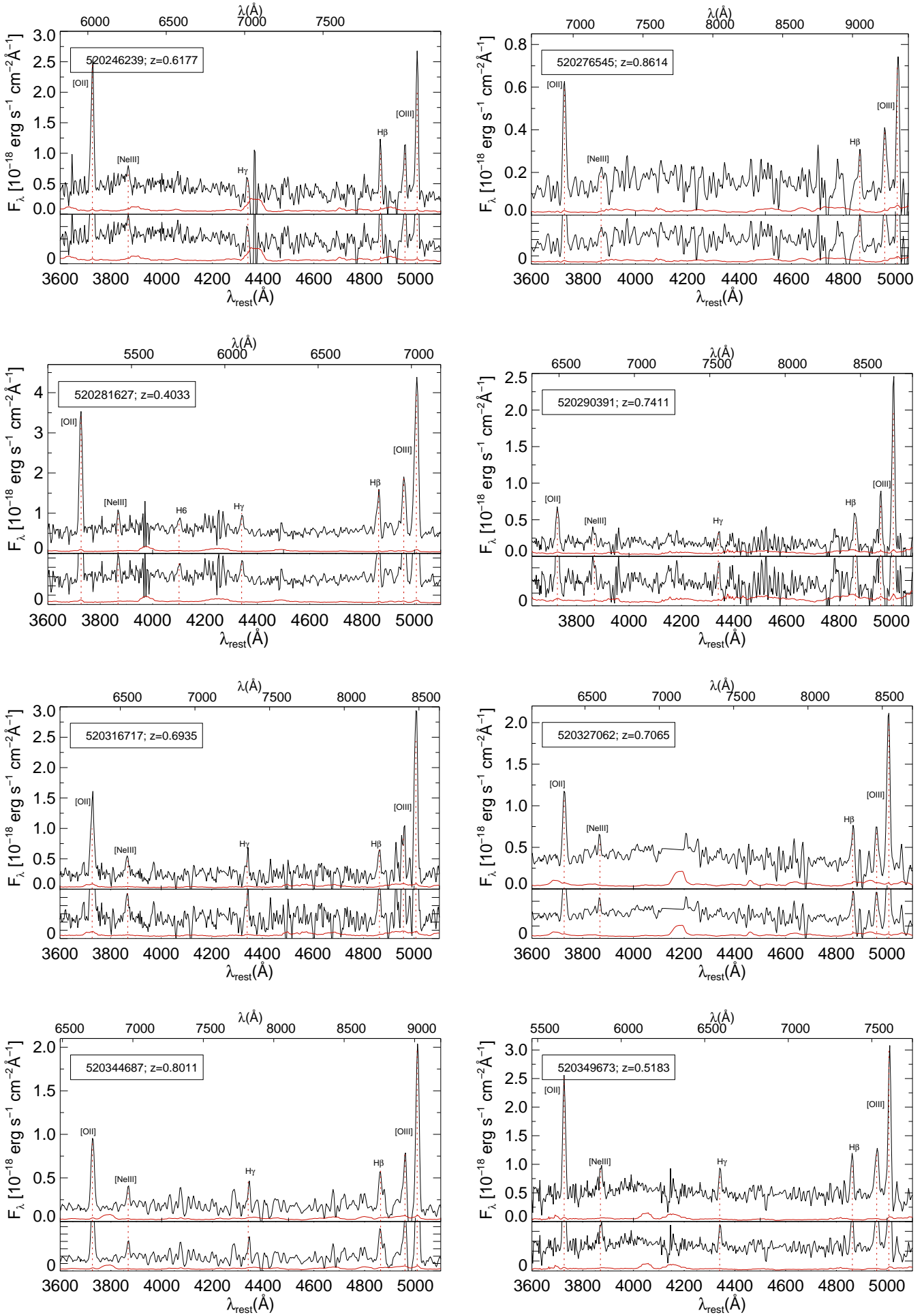


Fig. 1: VUDS spectra for the sample galaxies. A close-up version is shown in the bottom panel. The galaxy ID, redshift, and the main detected nebular emission lines are labeled. The 1σ noise spectrum is shown in red.

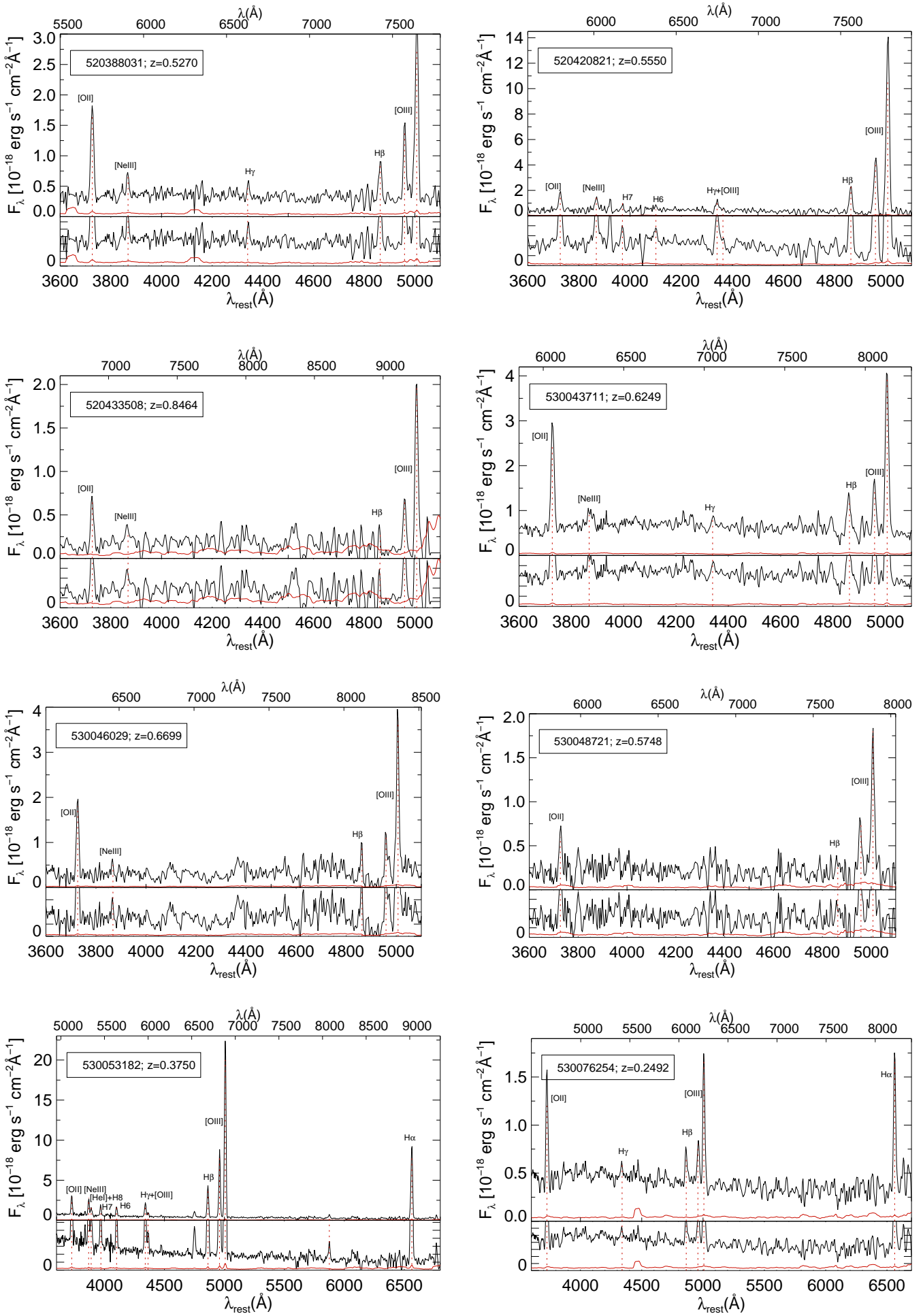


Fig. 1: VUDS spectra for the sample galaxies. Continued

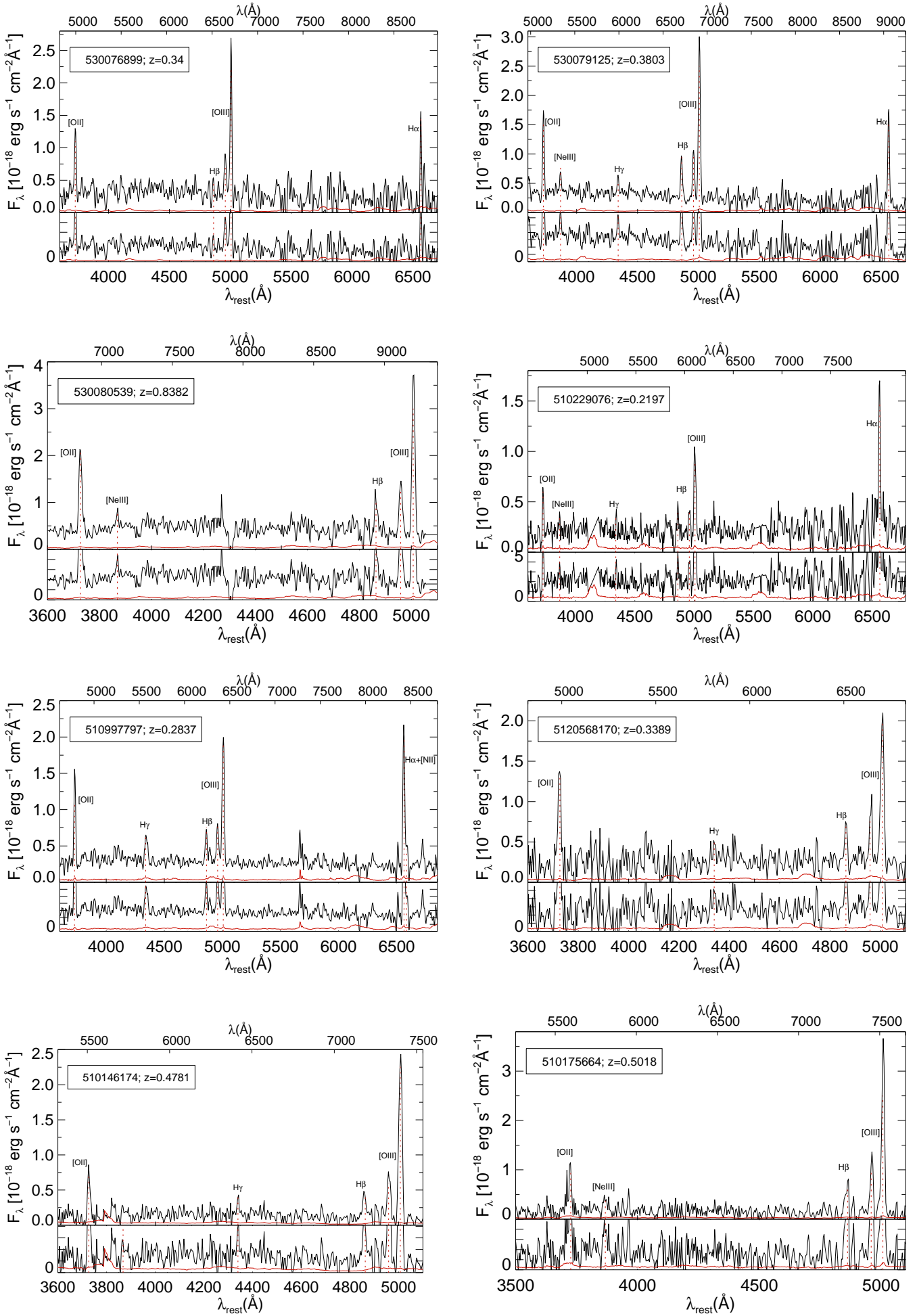


Fig. 1: VUDS spectra for the sample galaxies. Continued

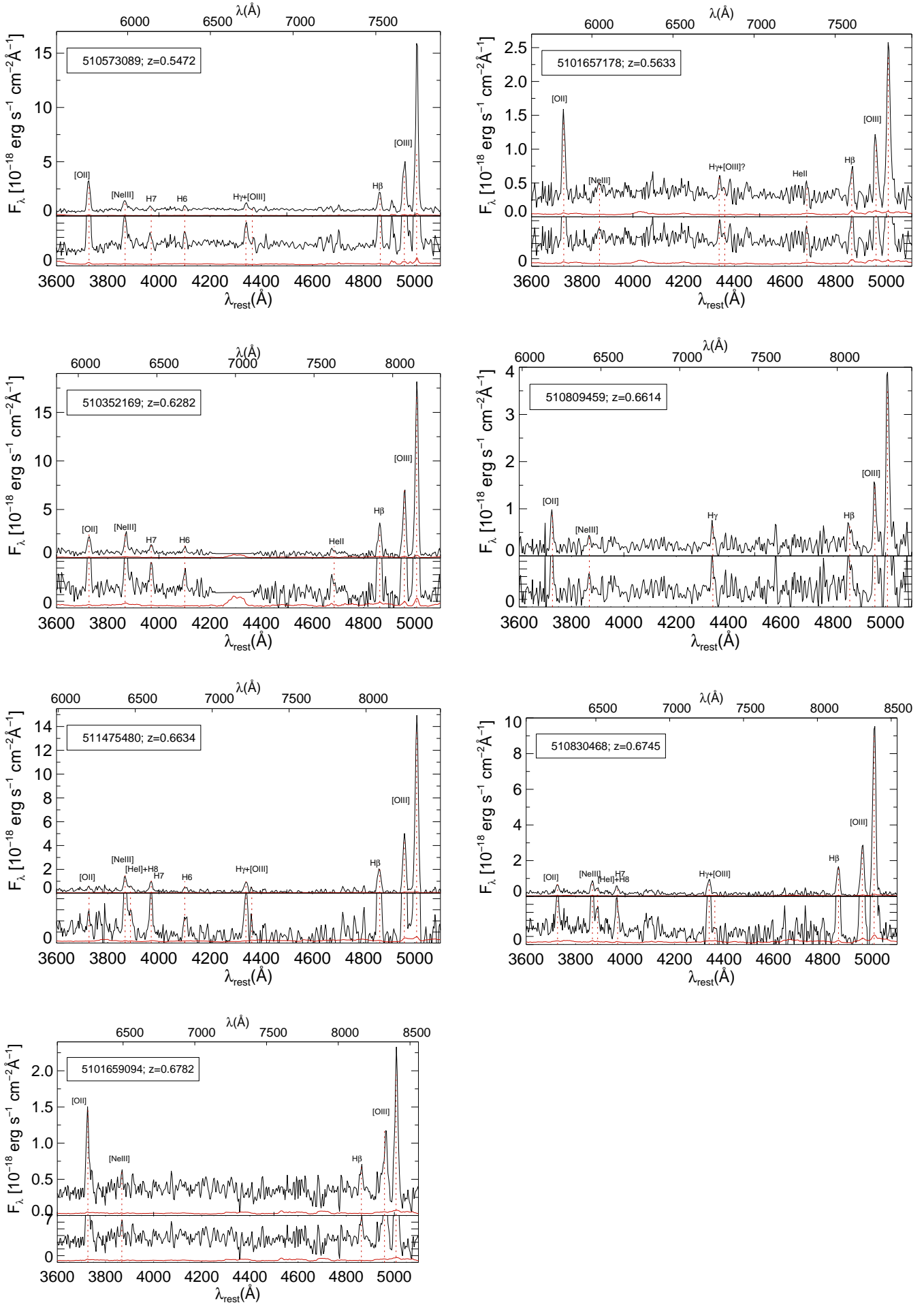


Fig. 1: VUDS spectra for the sample galaxies. Continued